

Random Chiral Asymmetry Generation by Chiral Autocatalysis in a Far-from-Equilibrium Reaction System

Kouichi Asakura,^{*,†} Akihito Ikumo, Kazuyuki Kurihara, and Shuichi Osanai

Department of Applied Chemistry, Faculty of Science & Technology, Keio University, 3-14-1, Hiyoshi, Kohoku, Yokohama 223-8522, Japan

Dilip K. Kondepudi^{*,‡}

Department of Chemistry, Wake Forest University, Winston-Salem, North Carolina 27109

Received: October 14, 1999; In Final Form: December 23, 1999

If the growth in a local concentration due to an autocatalytic process overcomes diffusion, a concentration fluctuation in a small volume will grow. In a chirally autocatalytic system, this phenomenon could produce a large variation in the enantiomeric excess (ee). Here we report kinetic studies that show such stochastic behavior in the synthesis of an autocatalytic chiral cobalt complex. The established values of the kinetic parameters indicate that temperature inhomogeneities in the form of local hot spots can have a significant effect on the progress of the reaction as well as the ee of the final product. Stochastic kinetics of this type are in stark contrast to deterministic kinetics that are usually encountered in chemistry; in these systems random fluctuations play an important role in determining the product distribution. In the present case we find large random fluctuations in the ee.

1. Introduction

In the well-known clock reaction, highly autocatalytic processes can make the reaction system suddenly change color with an almost clocklike accuracy. Under certain conditions, however, the chlorite–thiosulfate and chlorite–iodide clock becomes “crazy” and unpredictable.¹ The abrupt takeoff of the reaction is a growth in a fluctuation resulting from autocatalytic production of H⁺. In a small volume, a random increase in concentration of a species is countered by loss due to diffusion. But if the autocatalytic increase in concentration can overcome the loss due to diffusion, the random fluctuation will grow and drive the whole system to a state of high H⁺ concentration. Since the supercritical concentration fluctuations are random events, the induction period for each experiment varies randomly. The stochastic nature observed in the yield of the cobalt complex reported in this article is quite similar to the crazy clock phenomena.¹

Among autocatalytic reactions, chirally autocatalytic chemical reactions are of particular interest because they may shed some light on the possible origins of biomolecular homochirality.^{2–5} But the fact that these systems also show strong stochastic behavior is not generally appreciated. The stochastic behavior appears in the enantiomeric excess (ee) that these systems generate. Theoretical models that contain chirally autocatalytic steps, such as Frank’s model⁶ and Calvin’s model,⁷ show the possibility of spontaneous chiral asymmetry generation, i.e., the excess production of one enantiomer in a nonchiral environment. In these models each enantiomer of the chiral product, which can catalyze its own production, is generated either from achiral reactants or from racemic reactants that racemize rapidly. In such reactions, a random ee that may arise due to a local

fluctuation can rapidly grow and this process can result in stochastic behavior. In this article we present our study of such a system which involves the synthesis of a chiral cobalt complex.

In crystallizations of achiral or racemic compounds that crystallize in chiral forms random generation of chiral asymmetry can be observed.^{8–13} The Gaussian-like probability distribution for the ee of the product is observed in systems that are not chirally autocatalytic. If the solution or the melt is continuously stirred during crystallization, the chirally autocatalytic process of secondary nucleation dominates the system and, in this case, a bimodal probability distribution is observed for the ee.^{12,14} Larger than 90% ee occurs in each crystallization with equal probability for the excess being in either enantiomer; the ee of the product thus exhibits highly stochastic behavior.

Here we report the stochastic behavior in the synthesis of a chiral Co complex in which the autocatalysis is in the generation of the chiral molecule and not a crystal as in the above-mentioned cases. The stochastic variation in the ee of the Co complex is not as dramatic as in the case of crystallization but is significant.

2. Chirally Autocatalytic Kinetics

A trinuclear cobalt complex, [Co(H₂O)₂{(OH)₂Co(en)₂}]₂-(SO₄)₂ (**A**), reacts with NH₄Br (**B**) in aqueous media to produce a chiral octahedral cobalt complex, *cis*-[CoBr(NH₃)(en)₂]Br₂ (**D**). Our experiments¹⁵ have shown that the reaction proceeds through the intermediate complex [Co(H₂O)(OH)(en)₂]²⁺ (**C**); the ligand replacement of (OH)[−] and H₂O by NH₃ and Br[−] leads to the final stable chiral complex **D** as shown in Figure 1.¹⁵ Even though the intermediate **C** is always produced as a racemic compound, random preferential production of one enantiomer of the final product **D** was shown to spontaneously occur.¹⁶

Except for some specific cases, the absolute structure is not maintained in the ligand exchange reactions,^{17–20} indicating that

[†] E-mail: asakura@apple.keio.ac.jp.

[‡] E-mail: dilip@wfu.edu.

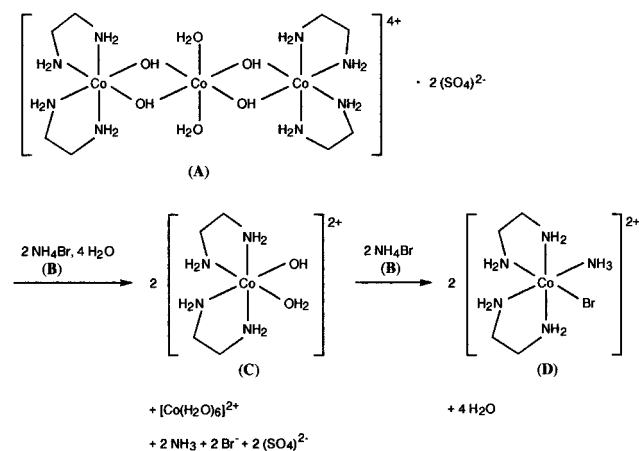


Figure 1. Preparation of a chiral octahedral cobalt complex, *cis*-[CoBr(NH₃)(en)₂]Br₂ (**D**).

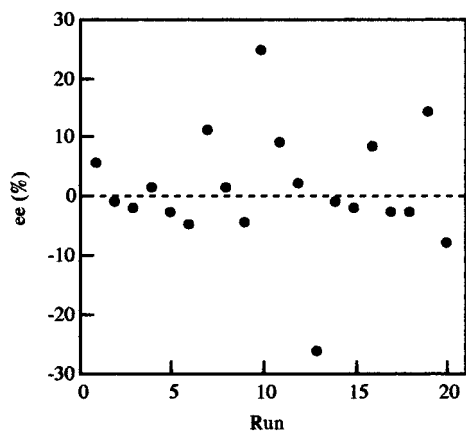


Figure 2. Randomly fluctuated ee of *cis*-[CoBr(NH₃)(en)₂]Br₂ (**D**) produced in the absence of seed crystals. Negative and positive values of ee respectively indicate the preferential production of levorotatory and dextrorotatory complexes.

the reaction from **C** to **D** proceeds through an achiral transition state. The chiral asymmetry generation thus seems to occur in the reaction from the achiral transition state to the product **D**.

A typical reaction is performed as follows. A reaction mixture consisting of 0.80 g of **A**, 4.00 g of **B**, and 4.0 mL of water is placed in a 50 mL reaction flask at 25 °C and stirred using a stir bar (2.5 cm in length, 0.8 cm in diameter) at 500 rpm. After 1 min, the flask is placed in a 50 °C water bath for 5 min. Finally, the product is isolated by passing the reaction mixture through cation-exchange resin chromatographic column (Sephadex SP C-25) using ammonium bromide aqueous solution as an eluent. For 20 experiments, the yield was found to be in the range 75–85% and the ee fluctuated from run to run as shown in Figure 2.

Yield and ee of the final product were obtained by the same method as described in our previous article.²¹ The concentration of **C** and **D** in the eluate was respectively determined by measuring the intensity of absorption at 512 and 542 nm of each eluate using a Hewlett-Packard 8452A spectrophotometer. Ten measurements were made for each eluate. The standard deviation was less than 1% of the average in every sample. Yields calculated from the volume and concentration of the eluate are thus trustworthy. Measurements using a Rudolph Research Autopol IV automatic polarimeter were also carried out for determining the optical rotation of each eluate. The standard deviation of the angle is less than 0.003° in every sample. All measurements were carried out having concentra-

tions at around $c = 0.1$ (g/100 mL) ($0.07 < c < 0.13$). Since the absolute value of specific rotation of enantio-pure **D** is $[\alpha]_{589} = 103^\circ$,²⁰ the angle of rotation of the sample having ee of 29.1% was 0.030° when $c = 0.1$. Thus the random variations of ee shown in Figure 2 are far above experimental error.

The chirally autocatalytic nature of this reaction could be clearly seen when enantiomeric crystals of the product are added to the reaction system.^{16,21} The product **D**, *cis*-[CoBr(NH₃)(en)₂]Br₂, crystallizes as a conglomerate; i.e., each crystal consists exclusively of one enantiomer (which is confirmed by the fact that solubility of racemic **D** was found to be twice that of the enantio-pure **D**).^{21,22} Addition of crystals of one enantiomer to the reacting solution results in the preferential production of that particular enantiomer as shown in Figure 3. In this case, 1, 3, 10, or 40 crystals in the size range 300–425 μm of (–)₅₈₉- or (+)₅₈₉-**D** were added to the reaction mixture in advance. Two kinds of stir bars, a small one having 1.2 cm in length and 0.5 cm in diameter and a large one having 2.5 cm in length and 0.8 cm in diameter, were used. We notice that an increase in the stirring rate and the use of a larger stir bar increase not only the average ee but also the magnitude of its fluctuations.

In interpreting these results, we assumed that the chirally selective synthesis of the product occurred on the surface of the added chiral crystals. In addition, in stirred systems, at high supersaturation, secondary crystals of the chiral product could originate in the vicinity of the crystals through the well-known process of secondary nucleation.²³ Assuming this mechanism, we could explain some of the observed stochastic generation of ee and its dependence on the stirring rate.²¹

However, our recent experiments show that this is not the only mechanism. Figure 4 shows the amount of the product, **D**, produced during the course of five repeated runs. The curves show large variations of 10–50% from run to run, the largest variations being in the early stages. As mentioned above, standard deviation of intensity of absorption at 542 nm for 10 repeated measurement was less than 1% of its average in each sample. The random fluctuation in yield of **D** experimentally obtained was thus not simply scatter due to measurement method.

The variation in the ee of the product as a function of the amount of product formed is shown in Figure 5. We found random chiral asymmetry could be generated even though the crystallization occurred after the reaction has virtually been completed, indicating that the presence of chiral crystal was not essential for the chiral autocatalysis. Not only yield but also ee was found to fluctuate by a large amount from run to run during the first 1 min of the reaction. This motivated us to investigate the system in greater detail and identify other mechanisms that may be the source of the observed stochastic behavior.

3. A Kinetic Model

To determine the mechanism of the observed large fluctuation in the yield and ee, kinetics of the reaction were carefully reinvestigated. The conversion of the intermediate, **C**, to the final product was monitored. The reaction was performed by adding 0.80 g of **A** into the mixture of 4.0 g of **B** and 4.0 mL of water (excess amount of **B** was added to keep the solution saturated with **B** throughout the reaction) in a 50 mL round-bottomed flask. The temperature of the mixture was kept at 40 or 50 °C throughout the reaction. A Teflon stir bar, of 2.5 cm length and 0.8 cm diameter, was used and the stirring rate was 500 rpm. The conversion of **C** to **D**, the final step of the reaction,

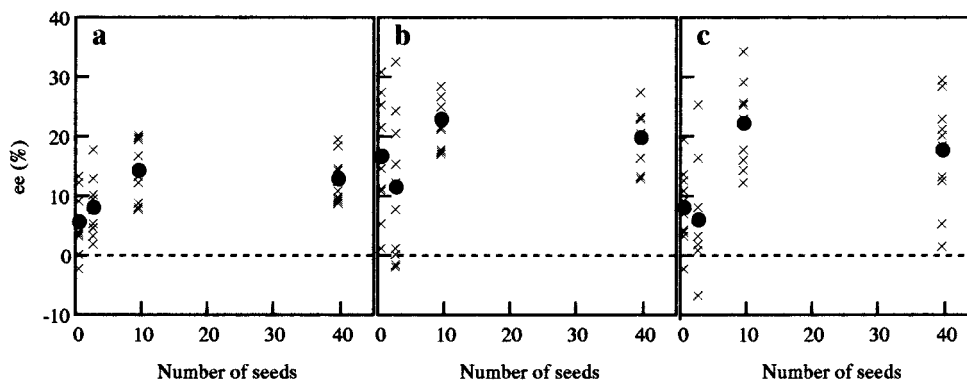


Figure 3. Distribution of ee of *cis*-[CoBr(NH₃(en)₂]Br₂ (**D**) produced under different stirring conditions. Negative ee indicates that the optical activity of the product is opposite to that of the seed crystals. Key: (a) small stir bar (1.2 cm in length, 0.5 cm in diameter), at 500 rpm; (b) small stir bar, at 1500 rpm; large stir bar (2.5 cm in length, 0.8 cm in diameter), at 500 rpm. Solid circles show the average ee.

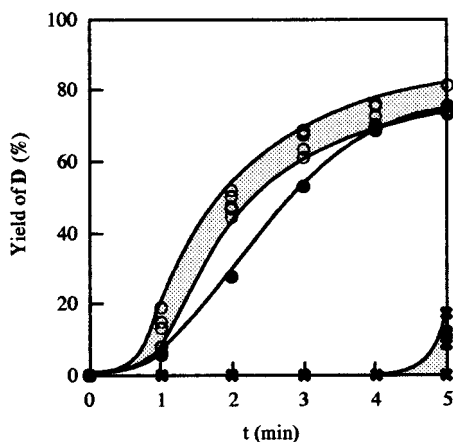


Figure 4. Change of the yield of **D**. The reaction mixture of 0.80 g of **A**, 4.0 g of **B**, and 4.0 mL of water in a 50 mL round-bottom flask was stirred for 1 min in 25 °C atmosphere and another 1–5 min in 50 °C water bath. A stir bar having 2.5 cm in length and 0.8 cm in diameter was used, and the stirring rate was 500 rpm. The x axis is the time after the flask was immersed into 50 °C water bath. The results of five times experiments (○) and a simulation (●) are shown. Amount of crystallized **D** was also determined and shown (×).

is expected to have a rate given by

$$\frac{d[\mathbf{D}]}{dt} = -\frac{d[\mathbf{C}]}{dt} = k[\mathbf{B}][\mathbf{C}] \quad (1)$$

Since **[B]** is in excess and does not change significantly during the reaction, the dependence of the rate constant *k* on product concentration **[D]** can be obtained by plotting $(1/[\mathbf{B}]) \ln[\mathbf{C}]/dt = -k$ as a function of **D**. To obtain the relationship between *k* and **[D]**, the plot shown in Figure 6, i.e., a plot of $\ln([C_0]/[C_t])$ vs time, was obtained at first. The data points are averages of three trials. The time derivative of this plot divided by **[B]** gives the value of *k*. A graph of $\ln([C_0]/[C_t])$ vs time at two reaction temperatures, 40 and 50 °C, is shown in Figure 6. On the same graph, the degree of supersaturation, $S = [\mathbf{D}]/[\mathbf{D}]_s$; in which **[D]_s** is the saturation concentration, is also plotted. Since the solubility of the product is relatively low, the concentration reaches supersaturation rather quickly. In the case of 40 °C reaction, the degree of supersaturation has the maximum at about 6.5 min, because the crystallization of **D** started 4.5–4.7 min after the reaction started.

To obtain the time derivative of $\ln([C_0]/[C_t])$, Mathematica was used to fit an analytical function to the curves in Figure 6, and the time derivative of this analytical function was used to obtain *k*.²⁴ In the calculation of $k = -(1/[\mathbf{B}]) \ln[\mathbf{C}]/dt$, the

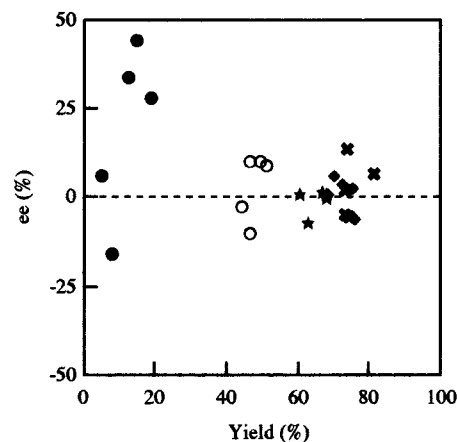


Figure 5. Change of yield and ee of **D** for five times experiments. The reactions for the results were same as the one for Figure 4. Results of each five times experiments for 1 (●), 2 (○), 3 (★), 4 (◆), and 5 (×) min reactions are shown. Negative and positive values of ee respectively indicate that levorotatory and dextrorotatory product are dominant.

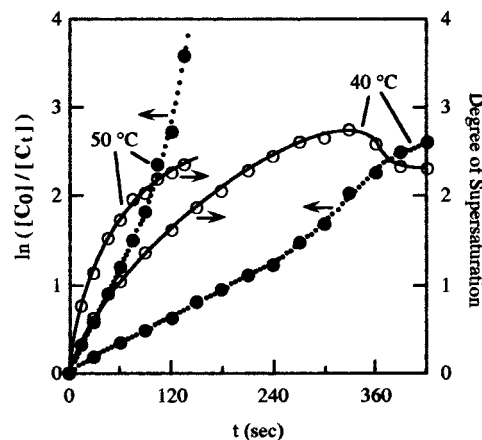


Figure 6. Change of $\ln([C_0]/[C_t])$ with time for the reaction at 40 and 50 °C (●). The function to represent the relationship between $\ln([C_0]/[C_t])$ and the time obtained by the Mathematica minimum square method is shown as a dotted line. The degree of supersaturation (*S*) of **D** at each time was also measured and shown (○).

values of **[B]** used were 9.16 and 9.97 M, when the reaction temperature was 40 and 50 °C, respectively. As can clearly be seen, the rate constant *k* increases with temperature, but more relevant to our discussion is the fact that it increases with increase of degree of supersaturation *S* of the product as shown in Figure 7. The rapid increase in the rate constant with the

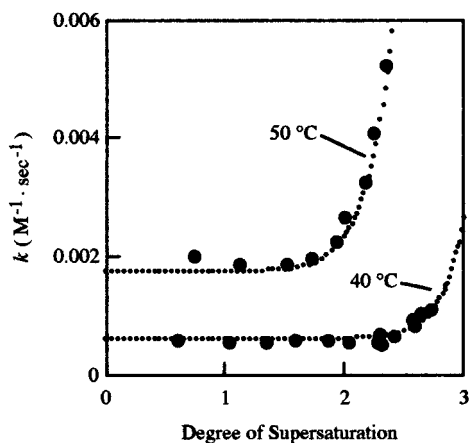


Figure 7. Relationship between the rate constant and degree of supersaturation (S) for 40 and 50 °C reactions. Functions obtained by the least-squares “NonlinearFit” package of Mathematica are shown as a dotted line.

increase in the product concentration shows the autocatalytic nature of the reaction. As can be seen in Figure 7, there seems to be an onset of autocatalysis when supersaturation exceeds a certain threshold value.

To quantify this autocatalytic nature of the reaction for modeling purposes, we have used a “cluster model”. In this model, we assume that as the supersaturation increases, the chiral product **D** forms enantiomeric clusters, i.e., each cluster consists of exclusively Λ -**D** or Δ -**D**. This assumption is consistent with the fact that **D** crystallizes as a conglomerate (each crystal is enantiomerically pure).^{21,22} When these clusters reach a critical size consisting of M molecules, they become chirally selective catalysts, thus making the reaction mechanism chirally autocatalytic.

For the formation of the clusters, we adopt the simple stepwise addition of monomers



in which the subscript n indicates the size of the cluster, n -mer. We assume that reaction 2 equilibrates rapidly and that the rate constant does not vary significantly with n so that

$$\frac{[\Lambda\text{-D}_{n+1}]}{[\Lambda\text{-D}_n][\Lambda\text{-D}]} = K \quad (3)$$

with a similar equation for the other enantiomer. It then follows that

$$\frac{[\Lambda\text{-D}_{n+1}][\Lambda\text{-D}_n][\Lambda\text{-D}_{n-1}] \cdots [\Lambda\text{-D}_2]}{[\Lambda\text{-D}_n][\Lambda\text{-D}_{n-1}][\Lambda\text{-D}_{n-2}] \cdots [\Lambda\text{-D}]} = [\Lambda\text{-D}]^n K^n$$

i.e.

$$[\Lambda\text{-D}_n] = [\Lambda\text{-D}]^n K^{n-1} \quad (4)$$

The total concentration of the Λ -catalyst, which we shall denote by \mathbf{X}_Λ , is the concentrations of Λ -clusters of size M or larger, which equals

$$\begin{aligned} [\mathbf{X}_\Lambda] &= \sum_{i=M}^{\infty} [\Lambda\text{-D}_i] = \sum_{i=M}^{\infty} [\Lambda\text{-D}]^i K^{i-1} = \\ &= \frac{[\Lambda\text{-D}]^M K^M}{K} \sum_{i=0}^{\infty} [\Lambda\text{-D}]^i K^i \quad (5) \end{aligned}$$

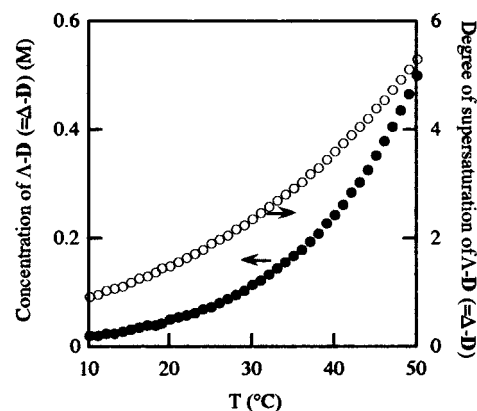


Figure 8. Critical concentration (●) and degree of supersaturation (○), at which the reaction suddenly takes off, as the function of temperature.

TABLE 1: Parameters of the Rate Constant Obtained Using the Least-Squares “NonlinearFit” Package of Mathematica

	50 °C	40 °C
M	9.86	11.99
k_2/K	2.825	0.0015
y	0.188	0.278

The term $[\Lambda\text{-D}]K$ will be less than 1 if $[\Lambda\text{-D}_{n+1}] < [\Lambda\text{-D}_n]$, which is generally true in normal supersaturated solution. Then (5) can be written as

$$[\mathbf{X}_\Lambda] = \frac{1}{K} \frac{[\Lambda\text{-D}]^M K^M}{(1 - [\Lambda\text{-D}]K)} \quad (6)$$

The rate constant k in eq 1 can now be written as

$$k = k_1 + k_2([\mathbf{X}_\Lambda] + [\mathbf{X}_\Delta]) \quad (7)$$

in which k_1 is the rate constant in the absence of the clusters and $[\mathbf{X}_\Lambda]$ is an expression similar to (6). If $[\Lambda\text{-D}] = [\Delta\text{-D}] = [\mathbf{D}]/2$, then expression (7) can be written in terms of the degree of supersaturation $S = [\Lambda\text{-D}]/[\Lambda\text{-D}]_S (= [\Delta\text{-D}]/[\Delta\text{-D}]_S)$ (in which $[\Lambda\text{-D}]_S$ and $[\Delta\text{-D}]_S$ are the saturation concentration) as

$$k = k_1 + \frac{2k_2}{K} \frac{S^M y^M}{(1 - Sy)} \quad y = [\Lambda\text{-D}]_S K (= [\Delta\text{-D}]_S K) \quad (8)$$

This expression for the rate constant can be used to fit the data in Figure 7 using k_1 , k_2/K , M , and y as parameters. Fitting the expression (8) using the least-squares “NonlinearFit” package of Mathematica to the data gave the values for the parameters shown in Table 1.

These parameters indicate that clusters of size about 10 or larger have catalytic activity. In addition, k_2 and K respectively are represented as the functions of temperature as

$$k_2 = 3.89 \times 10^{93} \exp(-6.91 \times 10^4/T) \quad (9)$$

$$K = 3.85 \times 10^{-10} \exp(7.23 \times 10^3/T) \quad (10)$$

Expression (8) indicates that the reaction is highly autocatalytic when Sy is close to 1. The critical concentration and degree of supersaturation, at which the reaction suddenly takes off, as the function of temperature can be calculated. The result is shown in Figure 8.

A comparison between the growth of the product **D** as a function of time given by the cluster model and the experimental data is shown in Figure 4. Though the theory qualitatively produces the shape of the growth curve of **D**, the quantitative

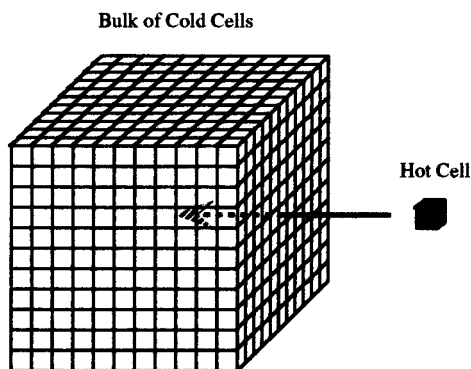


Figure 9. Model reaction system to investigate the influence of temperature and concentration inhomogeneity for a chiral autocatalytic reaction. A fragment of the hot part is thrown into the center of the cubic shaped bulk of cold cells.

fit is poor. Since the rate constants have been determined by their empirical dependence on the supersaturation, there is no room for altering them to fit the growth of **D**.

The observed discrepancy between the theory and experiment and the stochastic variation in **D** from run to run could be the result of local fluctuations in temperature and concentration that could grow rapidly. This is because, during the experiment, the reaction vessel was placed in an atmosphere at 25 °C with constant stirring for 1 min. Since the dissolution of **B** is endothermic, the temperature dropped to about 15 °C. Then the system was immersed into 50 °C water bath. Temperature inhomogeneity is thus likely to exist in the reaction system on a microscopic scale. The reaction proceeds faster in the hotter parts. Hence, if there are hot spots in the reaction vessel, the production rate can rapidly increase due to the autocatalytic nature of the reaction. This in turn increases the amount of **D** to a level greater than that expected on the basis of a homogeneous reaction. Indeed this is what we notice in Figure 4 when we compare the experimentally observed values of **D** with those predicted by the kinetic model.

If the thermal inhomogeneities can have significant impact on the growth rate of **D**, we should be able to demonstrate this possibility through a numerical simulation of the system with spatial inhomogeneities. To be more specific, a small thermal and concentration inhomogeneity should result in an local explosive growth of **D**. In the above model this can happen as follows.

Consider a case in which small reacting volume, dV , moves from a region of higher T into a region of lower T due to the mixing. At higher T , since the reaction rate and the supersaturation value of **D** are larger, the concentration of **D** will be larger than that in regions which are at lower temperature. When this volume dV moves into region at lower T and lower **D**, two processes begin to occur: (a) the conduction of heat from dV , which will decrease the temperature, and (b) the diffusion of **D** out of dV because the surrounding volume has a lower concentration of **D**. The decrease of T due to conduction will increase the supersaturation and hence the rate of autocatalytic production of **D** through cluster formation. On the other hand, the diffusion of **D** will decrease the concentration of **D** and decrease the rate of autocatalytic production of **D**. Rapid growth of **D** can occur only when the autocatalytic rate can take off despite diffusion. To see if this is possible, the following simulation was performed.

Our model consists of $11 \times 11 \times 11$ cells having temperature of 20 °C, which exchange matter through diffusion and heat through conduction as show in Figure 9. The volume of each

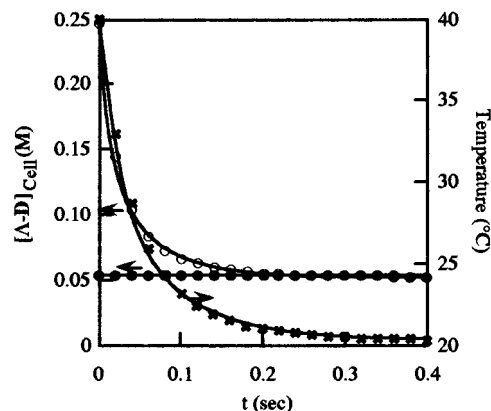


Figure 10. Computer simulation of change of the concentration of Λ -**D** (O) and the temperature (\times) in a 40 °C cell (volume: $(0.2 \text{ mm})^3$) when it is moved to a 20 °C environment. When the concentration Λ -**D** is above that shown by \bullet , an explosive growth of **D** can occur in the cell. (The condition for explosive growth is $S_y = 1$.)

cell was assumed to be $(0.2 \text{ mm})^3$. The diffusion rates and the conductivity were chosen to correspond to the experimental conditions.²⁵ A fragment of hot part (40 °C) having the same volume as a cold cell (20 °C), was then thrown into the very center of the array of cells at 20 °C. Since the yield and ee of **D** was observed to randomly fluctuate from trial to trial in a reaction run for 1 min, in a 50 °C water bath (Figures 4 and 5), the above-mentioned fragmentation of hot part into cold part can occur 45–55 s after the flask was immersed into the bath. The simulation was thus carried out to monitor the production of **D** in the hot cell, which was kept at 40 °C for about 50 s and then moved to a region surrounded by cells at $T = 20$ °C.

The temperature of the hot cell thrown into the cold bulk dropped very rapidly while the concentration scarcely decreased. Consequently, the autocatalytic rate grew explosively so that the product S_y in eq 8 was nearly equal to 1. This happened in less than 0.3 s. In obtaining the expression (8) for the rate constant k , it was assumed that $S_y < 1$. At very high S , this assumption breaks down, and a different expression is to be used for k ; it only means that if $S_y > 1$, the autocatalytic growth rate is very high. In fact, we could adopt the criterion that, when $S_y = 1$, an explosive autocatalytic growth occurs. Figure 10 shows the change in T and the concentration of **D** as a function of time. In it, the value of the concentration of **D** above which explosive growth can occur is also shown.

Thus large enhancements in the local growth of **D** can happen due to the autocatalytic nature of this system. This will increase the overall yield of **D** and could possibly be the reason for the observed difference (in Figure 4) between the theory and experiment. The quantitative aspects of this difference and stochasticity are beyond the scope of the current model. Because the system is also chiral autocatalytic, small differences in ee will also be amplified and will result in a random distribution of ee.

4. Concluding Remarks

When autocatalytic growth in the reaction system overcomes diffusion, the system may behave in a very unpredictable manner: large randomness may result in the time the reaction takes to reach a certain stage or in the product distribution.^{26–29} When there is chiral autocatalysis, there will also be fluctuations in ee. This observation must be borne in mind when a large ee is observed in some process. For example, an unexpectedly large ee in L-amino acids was recently found in the Murchison meteorite.^{30,31} If the observed ee is due to a chiral autocatalytic

process, we may expect large fluctuations in enantiomeric excess in different parts of the meteorite. Conversely, if large fluctuations in ee are found, it may be considered a signature of a chirally autocatalytic process. A careful study of the amino acid ee in different parts of a meteorite is yet to be done.

Acknowledgment. We are grateful for a Grant-in-Aid for Encouragement of Young Scientists from the Ministry of Education, Science, Sports, and Culture in Japan and a grant from the Amano Institute of Technology. One of us (D.K.) thanks the NSF (Grant CHE-9527095) for supporting this work.

References and Notes

- (1) Nagypál, I.; Epstein, I. R. *J. Phys. Chem.* **1986**, *90*, 6285.
- (2) Mason, S. F. *Nature* **1984**, *311*, 19.
- (3) Hegstrom, R.; Kondepudi, D. K. *Sci. Am.* **1990**, *262*, 108.
- (4) Bonner, W. A. *Origins Life Evol. Biosphere* **1991**, *21*, 59.
- (5) Bonner, W. A. *Origins Life Evol. Biosphere* **1994**, *24*, 63.
- (6) Frank, F. C. *Biochim. Biophys. Acta.* **1953**, *11*, 459.
- (7) Calvin, M. *Chemical Evolution*; Oxford University Press: Oxford, U.K., 1969.
- (8) Havinga, E. *Biochim. Biophys.* **1954**, *13*, 171.
- (9) Powell, H. M. *Nature* **1952**, *170*, 155.
- (10) Green, B. S.; Lahav, M. *J. Mol. Evol.* **1975**, *6*, 99.
- (11) Okada, Y.; Takebayashi, T.; Hashimoto, M.; Sato, S.; Tamura, C. *J. Chem. Soc., Chem. Commun.* **1983**, 784.
- (12) Kondepudi, D. K.; Kaufman, R.; Singh, N. *Science* **1990**, *250*, 975.
- (13) Pincock, R. E.; Perkins, R. R.; Ma, A. S.; Wilson, K. R. *Science* **1971**, *174*, 1018.
- (14) Kondepudi, D. K.; Laudadio, J.; Asakura, K. *J. Am. Chem. Soc.* **1999**, *121*, 1448.
- (15) Asakura, K.; Inoue, K.; Osanai, S.; Kondepudi, D. K. *J. Coord. Chem.* **1998**, *46*, 159.
- (16) Asakura, K.; Kobayashi, K.; Mizusawa, Y.; Ozawa, T.; Osanai, S.; Yoshikawa, S. *Physica D* **1995**, *84*, 72.
- (17) Brown, D. D.; Ingold, C. K.; Nylom, R. S. *J. Chem. Soc.* **1953**, 2673.
- (18) Kruse, W.; Taube, H. *J. Am. Chem. Soc.* **1961**, *83*, 1280.
- (19) Nordmeyer, F. R. *Inorg. Chem.* **1969**, *8*, 2780, 1969.
- (20) Buckingham, D. A.; Olsen, I. I.; Sargeson, A. M. *J. Am. Chem. Soc.* **1968**, *90*, 6654.
- (21) Asakura, K.; Kondepudi, D. K.; Martin, R. *Chirality* **1998**, *10*, 343.
- (22) Nakagawa, H.; Ohba, S.; Asakura, K.; Miura, T.; Tanaka, A.; Osanai, S. *Acta Crystallogr. C* **1997**, *53*, 216.
- (23) Randolph, A. D.; Larson, M. D. *Theory of Particulate Processes*, 2nd ed.; Academic Press: San Diego, CA, 1988; Chapter 4.
- (24) The analytical function used to fit the data points for $\ln([C_0]/[C_t])$ vs time for the two temperatures are the following: $y = -3.95009 \times 10^{-2} + 4.02752 \times 10^{-2} \exp(x/60) + 2.41807 \times 10^{-2}x - 3.65290 \times 10^{-5}x^2 - 6.82338 \times 10^{-7}x^3 + 7.21272 \times 10^{-12}x^5 - 3.82764 \times 10^{-17}x^7 - 1.09633 \sin(x/60)$ (dotted line) for 40 °C; $y = -3.76827 \times 10^{-1} + 3.65579 \times 10^{-1} \exp(x/60) + 2.12077 \times 10^{-2}x - 1.55724 \times 10^{-3}x^{1.5}$ (dotted line) for 50 °C. The derivatives of these functions, $y = 2.41807 \times 10^{-2} + 6.71254 \times 10^{-4} \exp(x/60) - 7.30581 \times 10^{-5}x - 2.04701 \times 10^{-6}x^2 + 3.60636 \times 10^{-11}x^4 - 2.67935 \times 10^{-16}x^6 - 1.82721 \times 10^{-2} \cos(x/60)$ and $y = 2.12077 \times 10^{-2}x + 6.09299 \times 10^{-3} \exp(x/60) - 2.33585 \times 10^{-3}x^{0.5}$, were used to obtain k shown in Figure 7.
- (25) The concentration of each enantiomer, $[\Delta\text{-D}]$ or $[\Lambda\text{-D}]$, in a small volume, in which temperature has been kept at 40 and 20 °C for 50 s, was calculated to be 5.38×10^{-2} and 4.80×10^{-3} M, respectively. We use the order of magnitude value of the 5.0×10^{-6} (cm² s⁻¹) for the diffusion coefficient D for species **D** of the solution and 6.28×10^{-3} (J cm⁻¹ s⁻¹ K⁻¹) for the heat conductivity.
- (26) Kondepudi, D. K.; Buhse, T. In *Randomness in Nonequilibrium Chemical Systems. Facing the Uncertain*; Prigogine, I., Driebe D., Eds.; University Texas Press: Austin, TX, in press.
- (27) Epstein, I. R.; Nagypál, I. In *Spatial Inhomogeneities and Transient Behavior in Chemical Kinetics*; Gray, P., Baras, F., Borckmans, P., Scott, S. K., Eds.; Manchester University Press: Manchester, U.K., 1990; p 461.
- (28) F. Sagués, L. Ramirez-Piscina, J. M. Sancho, *J. Chem. Phys.* **1990**, *92*, 4786.
- (29) Epstein, I. R. *Nature* **1995**, *374*, 321.
- (30) Cronin, J. P.; Pizzarello, S. *Science* **1997**, *275*, 951.
- (31) Engel, M. H.; Macko, S. A. *Nature* **1997**, *389*, 265.